RESEARCH ARTICLE
Cytoskeleton, August 2013 70:439–452 (doi: 10.1002/cm.21121)

Isolation of Intraflagellar Transport Trains

Caterina Mencarelli,[1]* Aaron Mitchell,[2] Roberto Leoncini,[3] Joel Rosenbaum,[4] and Pietro Lupetti[1]*

[1]Department of Life Sciences University of Siena, Via Aldo Moro 2, 53100, Siena, Italy
[2]Duke University Medical Center, Internal Medicine Residency Program, Durham, North Carolina
[3]Department of Medical Biotechnologies, University of Siena, Via Aldo Moro 2, 53100 Siena, Italy
[4]Department of Molecular Cellular and Developmental Biology, Yale University, New Haven, Connecticut

Received 8 February 2013; Revised 14 May 2013; Accepted 10 June 2013
Monitoring Editor: Bruce Goode

The intraflagellar transport (IFT) system was first identified in situ by electron microscopy in thin sections of plastic-embedded flagella as linear arrays of electrondense particles, located between the B tubules of the outer doublets and the flagellar membrane. These arrays of particles are referred to as IFT trains. Upon membrane rupture, IFT trains are thought to easily dissociate to yield soluble IFT particles, which are commonly purified through sucrose gradients as ~16-17S complexes. The latters easily dissociate into two subcomplexes, named A and B. We report here the isolation, visualization, and identification by immunolabeling of flexible strings of IFT particles, which are structurally similar to in situ IFT trains and appear to be formed by both complex A and complex B polypeptides. Moreover, the particles forming isolated IFT trains are structurally similar to the individual particles found in the ~17S gradient peak. Our results provide the first direct evidence that ~17S particles do indeed compose the IFT trains. The paper also represents the first isolation of the IFT trains, and opens new possibilities for higher resolution studies on their structure and how particles are attached to each other to form the particle trains.

Key Words: IFT trains and particles; immunoelectron microscopy; negative staining

Introduction

Cilia and flagella are dynamic microtubule-based organelles that are exposed on the surface of most eukaryotic cells where they serve motility and sensory functions. They are structurally and functionally dependent on the continuous bidirectional transport of precursors from the cell body to the flagellar tip, where assembly takes place, and of turnover products back to the cytoplasm. This process, first described in the biflagellate green alga *Chlamydomonas reinhardtii* [Kozminski et al., 1993], is known as intraflagellar transport (IFT).

IFT is based on a complex molecular machinery. The anterograde (base to tip) movement is driven by heterotrimeric members of the plus-end directed kinesin-2 family [Kozminski et al., 1995], while the minus-end directed cytoplasmic dynein 2 is responsible for the retrograde (tip to base) motility [Pazour et al., 1998, 1999; Porter et al., 1999]. In addition, a second motor, the homodimeric kinesin OSM-3, was found to cooperate with kinesin-2 in the assembly of *Caenorhabditis elegans* sensory cilia [Snow et al., 2004]. Both flagellar precursors—including axonemal [Qin et al., 2004; Hou et al., 2007], membrane [Huang et al., 2007], and signal transduction proteins [Qin et al., 2005]—and turnover products [Qin et al., 2004] are transported as cargoes of large multiprotein complexes, the IFT particles, which are formed by ~ 20 polypeptides [reviewed by Cole, 2003; Taschner et al., 2012]. Homologues of IFT proteins have been identified in several distantly related species, indicating that the general features of the IFT mechanisms have been remarkably conserved during eukaryotic evolution [Cole, 2003; Avidor-Reiss et al., 2004; Li et al., 2004].

Mutations affecting IFT components result in defects in ciliary structure/function. Anterograde IFT mutants exhibit severe phenotypes, which are all characterized by either the absence of cilia or the assembly of very short cilia [see for example Pazour et al., 2000; Deane et al., 2001; Follit et al., 2006]. On the contrary, mutations affecting the retrograde transport are often more compatible with a partial or even a complete assembly of the cilium which is, however, characterized by the presence of IFT particles accumulated either at the tip or in lateral bulges along the cilium [Pazour et al., 1998; Tsao et al., 2008; Absalon et al., 2008; Iomini et al., 2001, 2009]. Both ciliary motility and sensory function can be affected by IFT mutations. In humans,

*Correspondence to: Caterina Mencarelli; Department Life Sciences, University of Siena, Via Aldo Moro 2, 53100 Siena, Italy. E-mail: caterina.mencarelli@unisi.it (or) Pietro Lupetti; Department Life Sciences, University of Siena, Via Aldo Moro 2, 53100 Siena, Italy. E-mail: pietro.lupetti@unisi.it
Published online 7 August 2013 in Wiley Online Library (wileyonlinelibrary.com).

the crucial role of IFT in ciliary function has been recently highlighted by discoveries linking abnormalities in the development of different tissues and organs to the impaired signaling function of primary cilia, and to a number of pathologies that are now collectively indicated as ciliopathies [Badano et al., 2006; for recent reviews, see van Reeuwijk et al., 2011; Davis and Katsanis, 2012].

IFT particles are moved by the IFT anterograde and retrograde motors in the space between axonemal microtubules and the flagellar membrane, where they were first visualized as trains of electrondense particles. They are linked to the outer doublets by thin connections and, on the opposite side, are tightly associated with the inner surface of the flagellar membrane [Kozminski et al., 1995; Pedersen et al., 2006; Pigino et al., 2009].

Structural analysis of IFT particles has not progressed rapidly. All the available in situ structural information comes from electron microscopic analyses of IFT trains carried out on resin-embedded samples [Kozminski et al., 1995; Pigino et al., 2009]. Recently, it has been shown that two categories of IFT trains occur in *Chlamydomonas* flagella: long trains (mean length about 700 and a 40 nm repeat) and short, more compact trains (mean length about 250 and a 16 nm repeat). Long and short trains have been proposed to be related to anterograde and retrograde movement, respectively [Pigino et al., 2009]. Thus, the shift from antero- to retrograde movement which occurs at the ciliary tip may involve the structural reorganization of IFT train components. Electron tomographic analysis of the long IFT trains in situ has clearly shown the occurrence of a regular repeat of IFT particles along the train as well as the presence of connections linking IFT particles to each neighboring one and to both the flagellar membrane and the B-tubule of axonemal doublet [Pigino et al., 2009].

Biochemical analyses and X-ray diffraction of crystallized IFT polypeptides have provided information about the protein composition of IFT particles, the interaction occurring between different IFT polypeptides and the high resolution structure of single and pairs of IFT polypeptides. When released from isolated flagella by detergents or freeze-thaw procedures IFT polypeptides have been shown to be associated in two complexes, named A and B, separable on sucrose gradients and columns [Cole et al., 1998; Lucker et al., 2005]. Complex A has a molecular mass of about 750 kDa and consists of six polypeptide subunits, which are named according to their molecular weight (IFT144, IFT140, IFT139, IFT122, IFT121, IFT43), while complex B has a predicted mass of about 1 MDa and consists of 14 subunits (IFT172, IFT88, IFT81, IFT80, IFT74, IFT72, IFT70, IFT57, IFT52, IFT46, IFT27, IFT25, IFT22, and IFT20). The genes encoding most IFT polypeptides have been cloned and found to contain sequence motifs involved in protein–protein interactions [reviewed by Cole, 2003]. The homology of IFT proteins to components of COPI coats and chlathrin vesicle coats has been reported [Avidor-Reiss et al., 2004; Jekely and Arendt, 2006 ; van Dam et al., 2013]; on this basis, it has been proposed that the IFT process evolved as a specialized form of coated vesicle transport from a protocoatomer complex. This hypothesis is corroborated by the involvement of IFT components in vesicle transport and exocytosis in cells not expressing a primary cilium [Finetti et al., 2009; Baldari and Rosenbaum, 2010].

Direct interaction between IFT polypeptides has been demonstrated within some pairs of complex B subunits [Baker et al., 2003; Wang et al., 2009; Fan et al., 2010; Lucker et al., 2005, 2010; Taschner et al., 2011], and the crystal structure of the IFT25/IFT27 dimer has been recently determined [Bhogaraju et al., 2011]. In addition, a model for the spatial arrangement of polypeptides within complex A has been proposed [Behal et al., 2012].

There is a large gap between the information provided by in situ ultrastructural studies and that provided by the molecular and biochemical analysis of IFT polypeptides. Complexes A and B have been related, respectively, to retrograde and anterograde movements [reviewed by Ishikawa and Marshall, 2011], however, we do not know if the two complexes are part of the same structure or how they are arranged within IFT trains. Finally, a detailed high resolution ultrastructural analysis of unfixed, unembedded IFT trains is still missing. A prerequisite for a high resolution structural study of single IFT particles and IFT trains is their isolation in their native form. We describe here, for the first time, the purification and visualization of IFT particles that are still associated to form flexible strings of particles and appear similar to IFT trains in situ. We show unequivocally by immunolabeling that the strings of isolated particles are indeed composed of IFT polypeptides, and that they are formed by both complex A and complex B proteins.

Results

Visualization and Identification of IFT Trains In Situ by Negative Staining and Immunolabeling

Disorganized piles of beaded structures were previously found to be associated with and to spread out from the axoneme tip after lysis of the flagellar membrane and negative staining of whole-mount flagella [Pedersen et al., 2005; Dentler, 2005]. These flagellar components were suggested to comprise IFT particles. We started our analysis on isolated IFT particles by reproducing this approach, with the aim of unequivocally establishing that the particles associated with the flagellar tip in earlier studies are indeed IFT particles.

In order to remove the flagellar membrane and to expose the underlying IFT components while preserving their in situ structural organization, we exposed cells to detergent for very short times in the presence of variable concentrations of

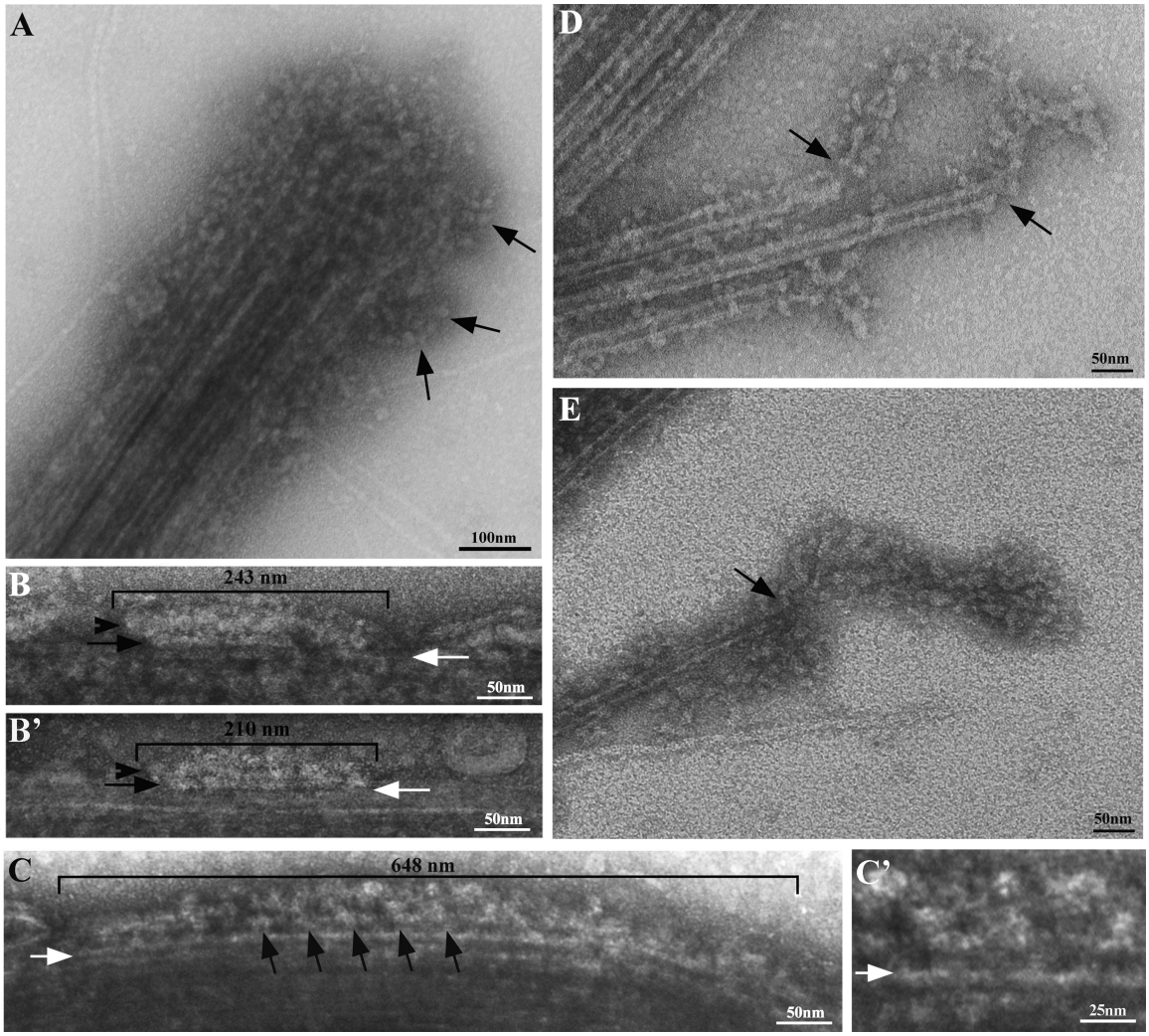

Fig. 1. Negative staining of in situ IFT particles. A. After treatment with 0.1% glutaraldheyde and 0.1% NP-40, the axoneme tip is compact and still embedded in a mass of roundish particles; a few strings of particles project laterally from the tip (arrows). **B–B'**, **C**. After demembranation in the presence of glutaraldheyde, linear arrays of particles are still associated with the side of the axoneme; their length and organization are compatible with those previously described for either short or long IFT trains [Pigino et al., 2009]. B–B'. Short arrays of particles are indicated by a bracket over which the length of the array is reported. The black arrows indicate the longitudinal domain present in the short arrays only, which is located between particles and the microtubule surface. Arrowheads indicate the thread of IFT particles located between the rod-like domain and membrane remnants. C. A long array of particles (bracket). The length of the array is indicated. Arrows point to the regular patterning of particles that is more clearly visible in the middle part of the array. The latter region is shown at a greater magnification in **C'**. White arrows in B–B', C–C' mark the microtubular surface. Images are oriented so that the tip of flagellum points to the left of the plate. **D–E**. At lower fixative and detergent concentrations (0.04% glutaraldehyde and 0.05% NP-40), the axoneme tip is partly disorganized and microtubule doublets splay onto the grid, showing strings of particles associated with the end of the tubule (arrows).

fixative. At higher fixative concentrations (0.1–0.5% glutaraldheyde, 0.1% NP-40), the axoneme tip is embedded in a massive amount of particles (Fig. 1A). Strings of roundish particles that are connected to each other by thinner links protrude laterally from the tip (arrows in Fig. 1A). Under these conditions, arrays of particles can be sometimes observed along the axoneme on the microtubule surface (Figs. 1B, 1B' and 1C). The length of these arrays is compatible with that reported for either short (retrograde) or long (anterograde) IFT trains [Pigino et al., 2009]; representatives of the two categories are shown in Figs. 1B, 1B' and 1C, respectively.

Retrograde, short IFT trains were previously described in sections from plastic-embedded flagella as arrays of tightly packed particles [Pigino et al., 2009]; similarly, the short structures that can be visualized along the axoneme by negative staining exhibit a compact and polarized organization, in which particles are not easily discernable as single entities but rather form a sort of thread located below remnants of flagellar membrane and glycocalyx (arrowheads in Figs. 1B and 1B'). Particles in short IFT trains are located on top of a rod-like structural domain, parallel to the microtubule surface (black arrows in Figs. 1B and 1B'). Such a rod-like domain is not visible in the long IFT trains.

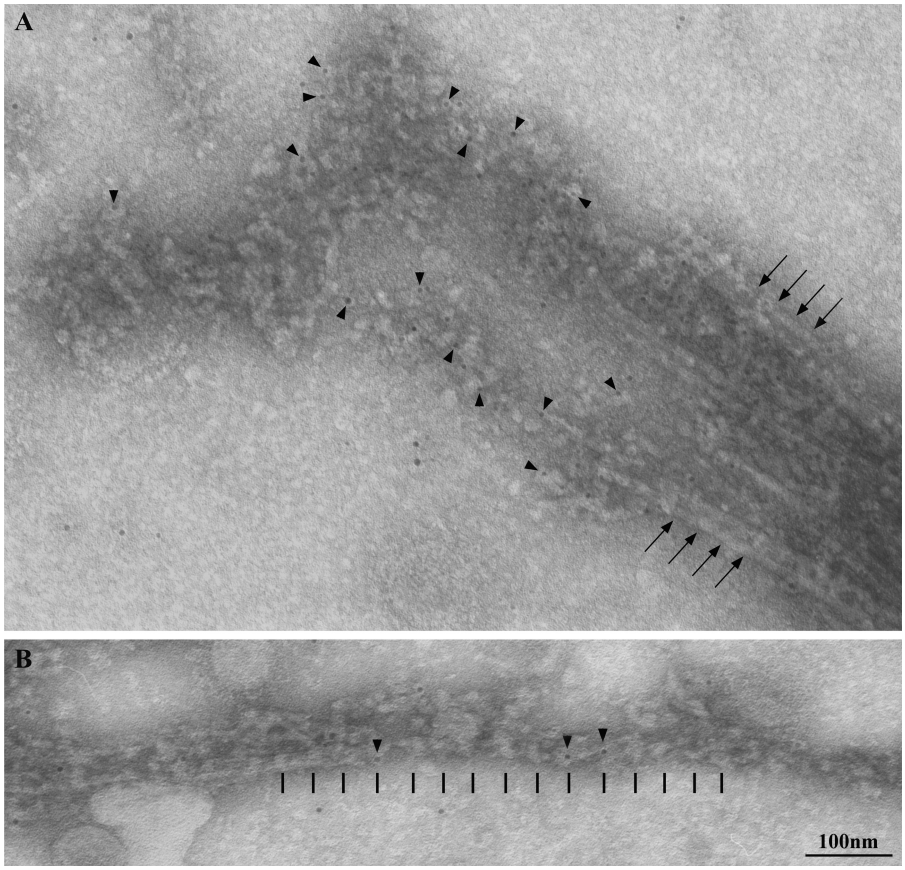

Fig. 2. Immunogold labeling of axoneme-associated IFT particles. A. Gold labeling is specifically localized on the particles that are associated with the axoneme tip. Arrowheads point to some of the gold particles; arrows indicate microtubular doublets. **B**. Linear strings of particles interconnected by oblique links are visible at the A tubule tip. The periodicity of the string shown here is about 38 nm, which is close to the one reported for the anterograde trains in situ (40 nm). Immunolabeling in A and B has been obtained with the complex A-specific antibody IFT 139.

Anterograde, long IFT trains appear as looser structures in which roundish particles are more easily detectable, close to the axoneme and interconnected by links (Figs. 1C and 1C'), in an arrangement that is strongly reminiscent of the one described by Pigino et al. [2009]. The 38–42 nm measured distance between adjacent particles is compatible with the 40-nm periodicity exhibited by long trains in flagellar sections from flat embedded cells [Pigino et al., 2009].

These observations suggest that the structural features of the IFT system are at least partly conserved during this procedure of fixation and membrane removal. If lower concentrations of both fixative and detergent are employed (0.04% glutaraldehyde 0.05% NP-40), particles are found to be less densely packed at the flagellar tip where the structure of the microtubules is also partly altered. This milder treatment allowed us to observe more easily individual strings of particles, in some instances emerging from the microtubule tip (Figs. 1D and 1E). For this reason, we used the latter gentle extraction/fixation conditions to carry out immunogold labeling experiments on whole-mount flagella using the IFT139 antibody, which is specific for the 139 kDa subunit of complex A. Under mild extraction conditions, gold particles specifically localize on the piles of particles associated with the tip (Fig. 2A). The axonemal tip splays onto the grid and axonemal microtubules, particularly the less stable central pair singlets, partially depolymerise.

Despite this partial loss of axonemal organization, it is possible to observe labeled linear arrays that are still associated with the microtubule end and display an almost regular patterning, consisting of ovoid particles, 26–28 nm × 16–17 nm in size, that are interconnected by oblique links, with a repeat of about 38 nm (Fig. 2B). This repeat is close to the one (40 nm) we observed in long trains [Pigino et al., 2009].

These data indicate that (i) IFT trains can be observed by whole-mount negative staining as strings of particles associated with the axoneme, (ii) these particles can be labeled by IFT-specific antibodies, (iii) the beaded structures associated with axoneme tips are indeed IFT particles in arrays of trains.

Isolation of Single IFT Particles and Trains of Particles from Gradients

In order to isolate IFT particles, we employed the basic sucrose gradient procedure designed by Cole et al. [1998] to purify IFT particles from *Chlamydomonas* flagella. Two

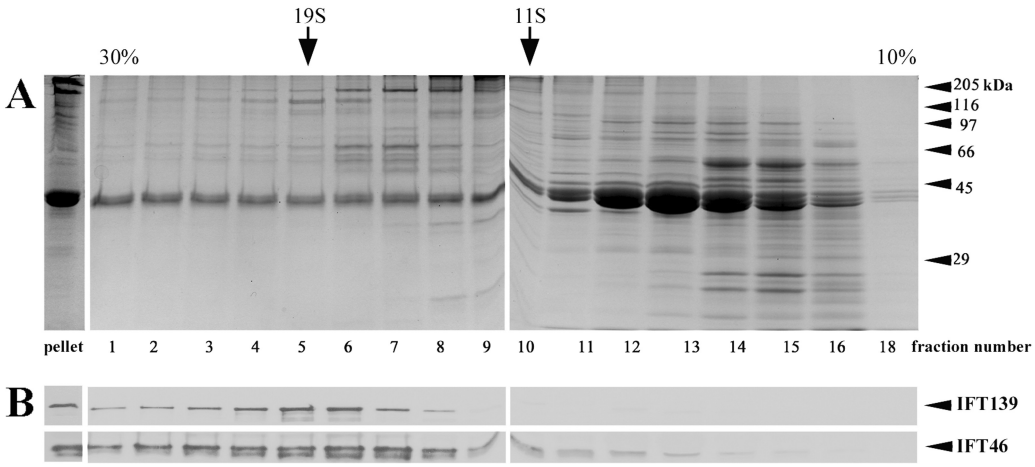

Fig. 3. Sucrose density gradient profile of the flagellar membrane plus matrix fraction. A. Coomassie blue staining. **B**. IFT139 and IFT46 immunostaining. Arrows mark the sedimentation position of thyroglobulin (19S) and catalase (11S); arrowheads indicate the electrophoretic migration of molecular weight standards (in kDa).

main changes were introduced in the preparation of the soluble (membrane and matrix) flagellar fraction, which were aimed at preserving the structural integrity of IFT particles and trains. First, based on the observation that the IFT trains are so tightly associated with the flagellar membrane [Pigino et al., 2009] the use of detergent might disrupt their organization even before gradient isolation, so no detergents were used. To gently disrupt the isolated flagella and to release both single particles and particle trains, a gentle procedure of freeze-thaw was used instead. Second, in order to allow the recovery not only of single IFT particles but also of heavier groups of IFT particles, i.e., trains, axonemes and partially disrupted flagella were removed after flagellar disruption by low speed centrifugations with no further clarification of the supernatant by high speed centrifugation (a high-speed centrifugation step was included in the preparation of the membrane + matrix flagellar fraction in previous studies on isolated IFT particles [see, e.g., Cole et al., 1998]. Finally, to improve the gold-labeling procedure and reduce background, the primary antibody labeling was carried out in solution, before gradient sedimentation of the low speed soluble supernatant (see M&M for details).

After gradient centrifugation and fractionation, the individual fractions were probed with antibodies to complex A (IFT139) and complex B (IFT46) polypeptides. Single IFT particles localized to the ~17S region of the gradient, as previously reported [Cole et al., 1998]. In addition, both IFT polypeptides also localized to a glassy pellet, which was found at the bottom of the gradient (Fig. 3). This suggested that the detergent-free, low-speed procedure we employed for IFT release permitted IFT particles to remain associated in larger and heavier complexes found at the bottom of the gradient. In addition, we inferred that IFT components could be associated with fragments of flagellar membrane in the glassy pellet because purified flagellar membranes show up as a glassy pellet (J. Rosenbaum personal communication).

To summarize, this fractionation procedure provided us with canonical ~17S IFT particles [Cole et al., 1998] and, most importantly, an additional fraction at the very bottom of the gradient, also enriched in IFT polypeptides and potentially a source of intact IFT trains.

Identification of Isolated IFT Trains in Negatively Stained preparations with Gold Labeled Antibodies

The gradient pellet was resuspended in buffer, negatively stained, and then analyzed by electron microscopy. It was found to contain roundish particles, frequently arranged into sinuous, flexible strings of variable lengths, which are often associated with what appear to be membrane vesicles (Fig. 4). The overall appearance of this material is quite similar to the IFT immunoreactive beaded structures associated with microtubule doublets detected in whole mount negatively stained axonemes (see Figs. 1 and 2). Particles were found to be arranged into single or double strings (arrows in Fig. 4A) or to form thread-like arrays (arrowheads in Fig. 4A; see also Fig. 4C for a higher magnification image). Frequently, they were associated with membrane patches or vesicles (white arrowheads in Figs. 4B and 4D).

IFT immunolabeling was specifically associated with the arrays of particles in the gradient pellet (Fig. 5A). When observed at a higher magnification, strings of particles appear to be labeled by both IFT139 (white arrows in Fig. 5B) and IFT46 (black arrows in Fig. 5B) antibodies. This finding clearly indicates that both complex A and complex B are present in the same string of particles.

Short regions showing an almost regular architecture consisting of two parallel strings of particles could be frequently observed, even within larger aggregates (see brackets in Fig. 5). Such a double arrangement of particles is a peculiar feature of the architecture previously described in anterograde IFT trains, where particles are interconnected by a double series of oblique links [Pigino et al., 2009].

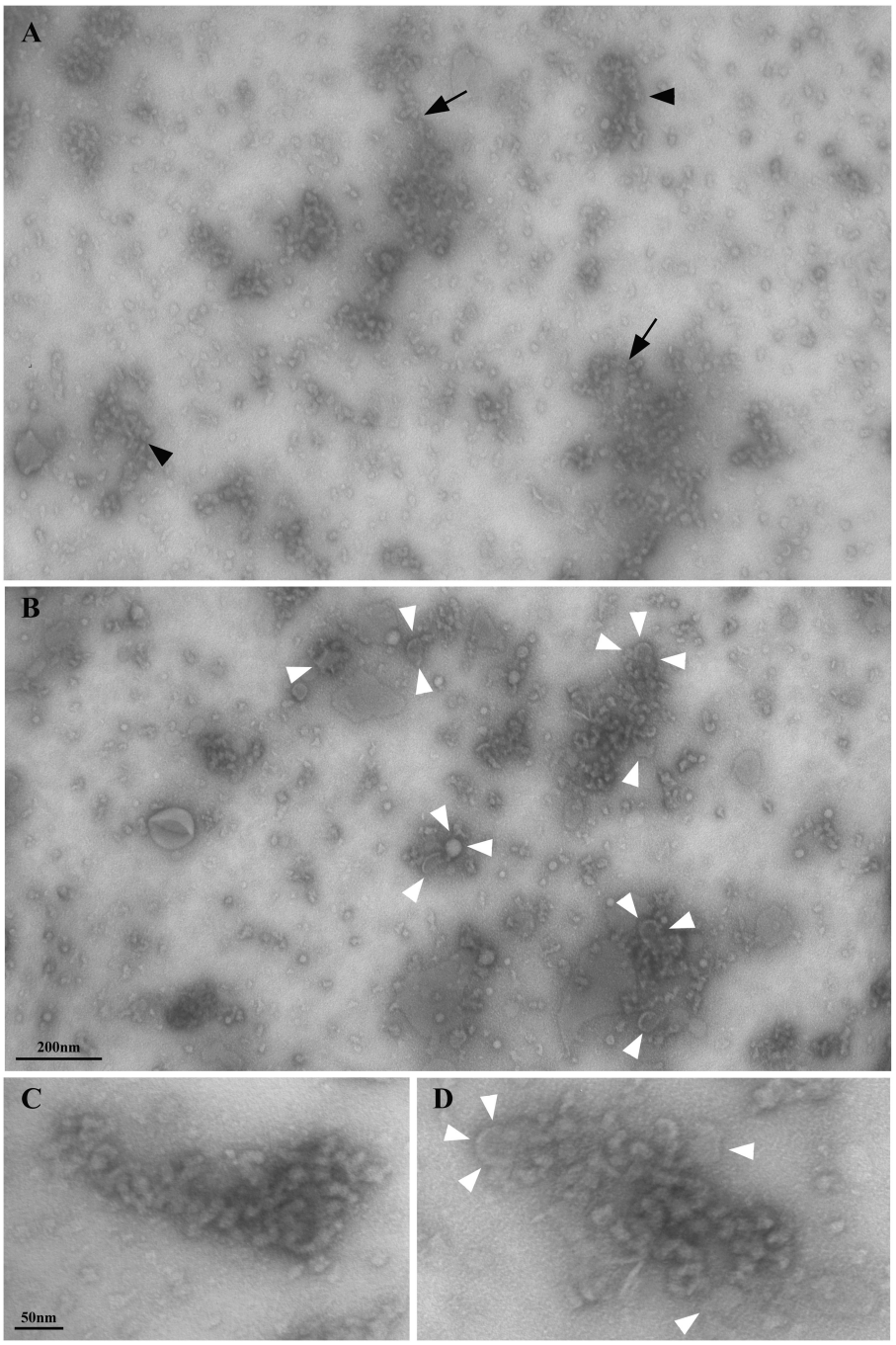

Fig. 4. A–B. Low magnification electron microscopy views of the material in the gradient pellet after negative staining, showing the presence of sinuous arrays of particles with different lengths and spatial arrangements. Arrows in A point to single strings of particles, while arrowheads indicate double strings or thread-like arrays of particles. In B the frequent association of particles with membrane vesicles (white arrowheads) is shown. Higher magnification views of two arrays of particles are shown in **C–D**; white arrowheads in D indicate membrane vesicles.

Oblique links could be discerned in either linear or double strings particle arrays, as exemplified in Fig. 6, where they are compared with the tomogram produced by Pigino et al.

To confirm the results obtained by negative staining of the IFT particles recovered in the gradient pellet, this pellet was also analyzed after plastic embedding and thin-sectioning. IFT particles appear in thin sections as electrondense particles, either arranged to form aggregates of variable dimensions or associated with membrane vesicles (Fig. 7A). Double rows of particles could be observed (brackets in Fig. 7B). Within this arrangement, particles may be disposed in a quite loose array, where they appear to be connected by links (arrows) or may be closer to each other forming a compact array (arrowhead). Depending on their orientation and on the plane of sectioning, some particles appear to possess a small cleft on one side (arrowheads in Fig. 7C).

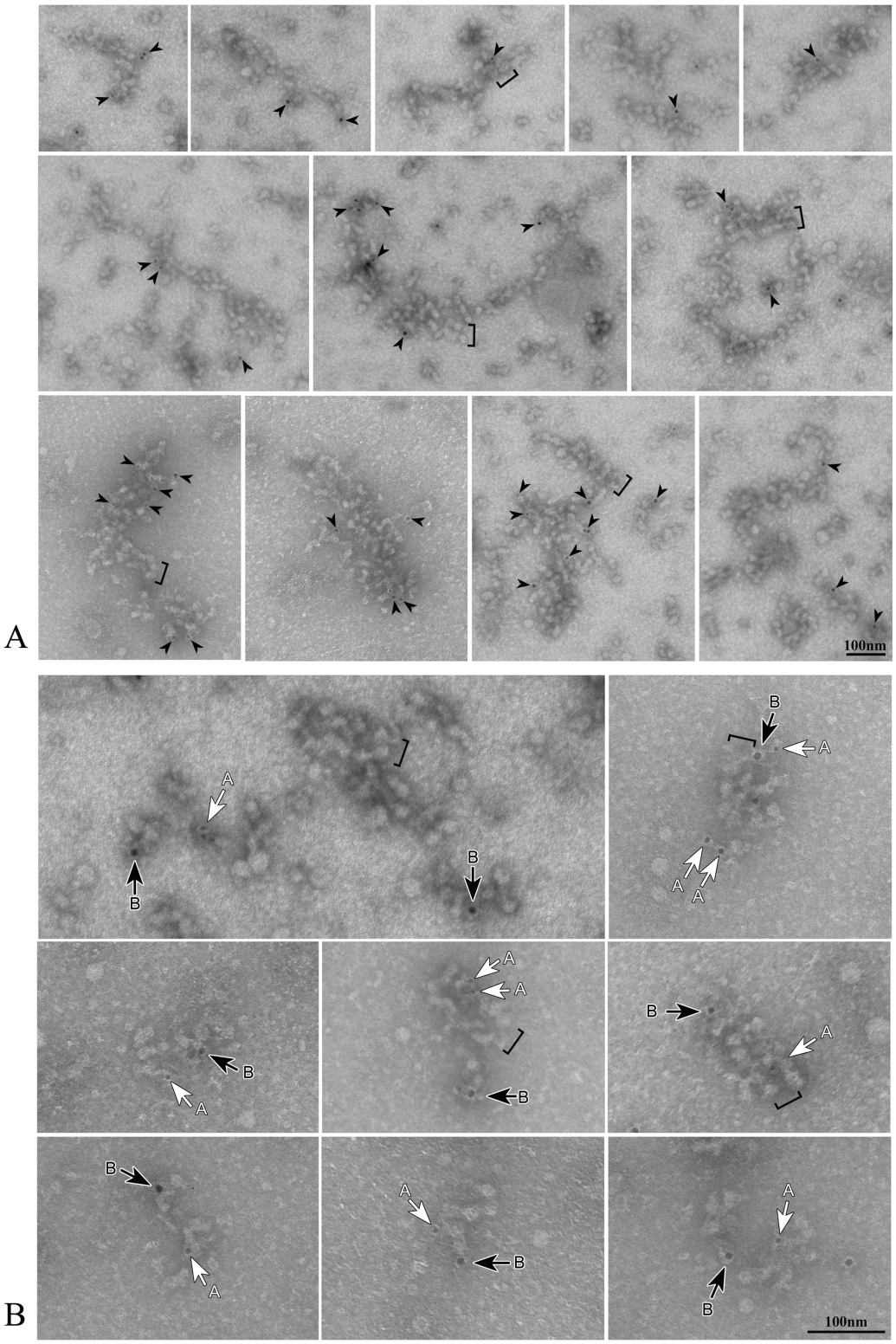

Fig. 5. A. **Isolated strings of particles are specifically labeled by IFT antibodies.** Gold particles have been indicated in this figure by arrowheads, without any distinction between complex A and complex B labeling. **B**. Both complex A (white arrows: IFT139, 5-nm gold) and complex B (black arrows: IFT46, 10-nm gold) antibodies react with IFT particle arrays. Brackets in both Figs. A and B indicate regions where particles are arranged in a double row.

Collectively, these data indicate that, provided the right isolation conditions are used, IFT trains do not completely dissociate after lysis of the flagellar membrane, but are released in solution as linear aggregates of particles that are likely to retain some of the structural features detected in IFT trains in situ.

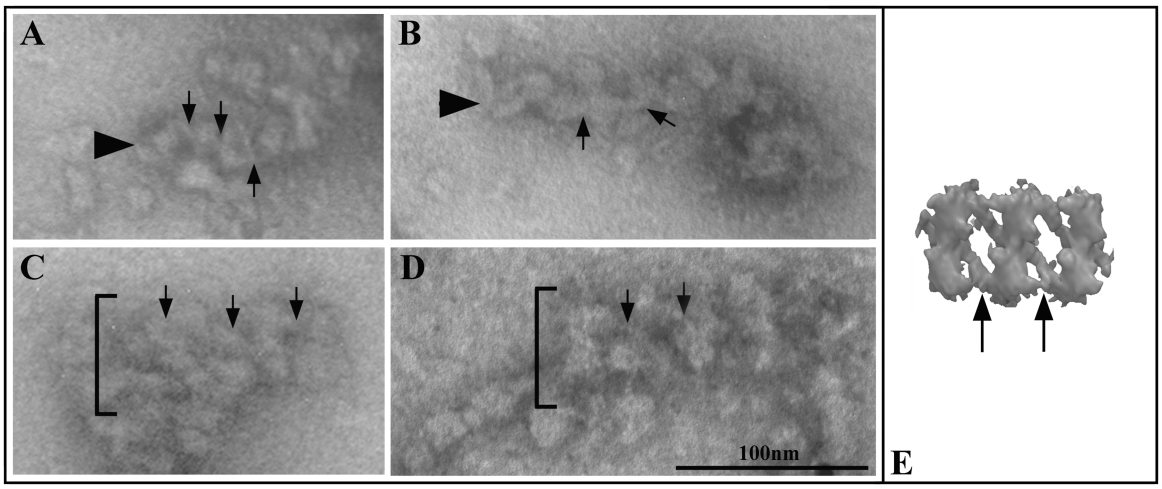

Fig. 6. Particles are connected by oblique links. These links are indicated by arrows in **A–E** and occur in both single string arrays (arrowheads in A–B) and double rows arrays (brackets in C and D). The tomogram obtained by Pigino et al. [2009] is shown in E for a comparison.

Isolated IFT Particles

We next analyzed the material in the gradient fractions at ~17S, which is expected to consist mainly of isolated particles. After gold-labeling and negative staining, these fractions were shown to contain particles—some of which were labeled—that exhibit a certain degree of structural variability and may be associated with each other into complexes of variable composition (Fig. 8). In order to analyze such structural heterogeneity, we classified labeled particles using a simple and straightforward morphometric approach, i.e.,

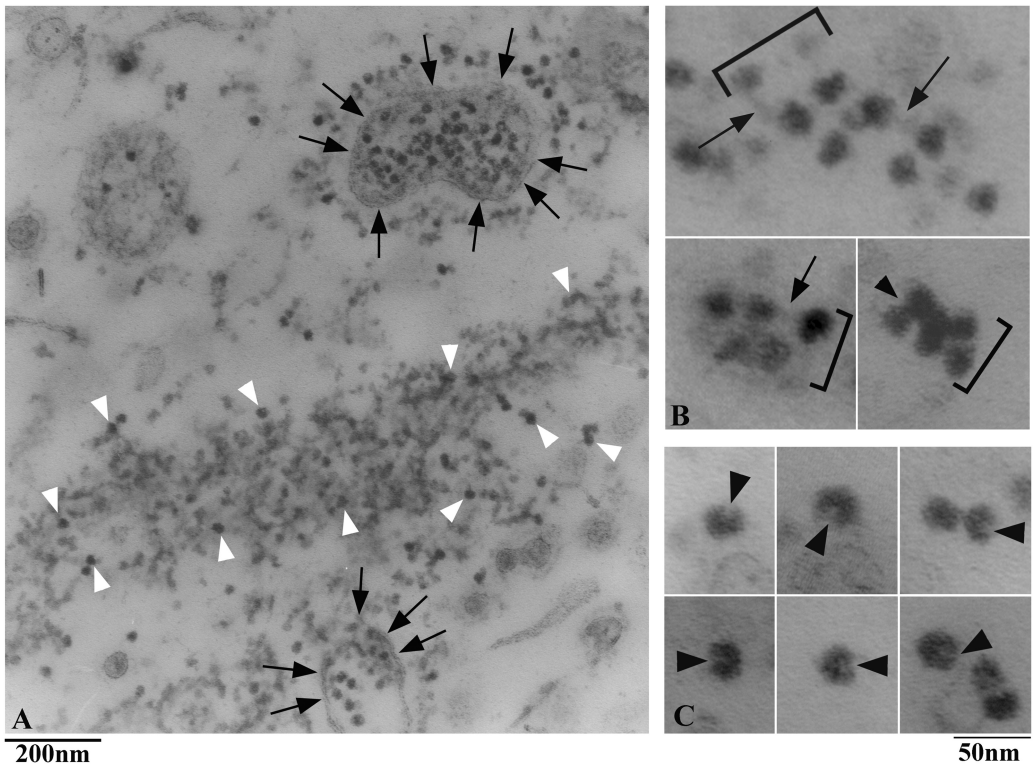

Fig. 7. Thin sections of the gradient pellet. A. Low magnification view. IFT particles appear as electrondense particles, some of which are here indicated by white arrowheads. Particles often associate to form large aggregates (as the one containing the particles indicated by the white arrowheads), or are associated with membrane vesicles (indicated by the black arrows). **B**. Higher magnification views of short, double row arrays of particles, which are indicated by brackets. The arrows indicate the interconnecting links between adjacent particles. The arrowhead indicate a double row array of particles showing a more compact organization. **C**. In some sections, particles appear to possess a central cleft (arrows).

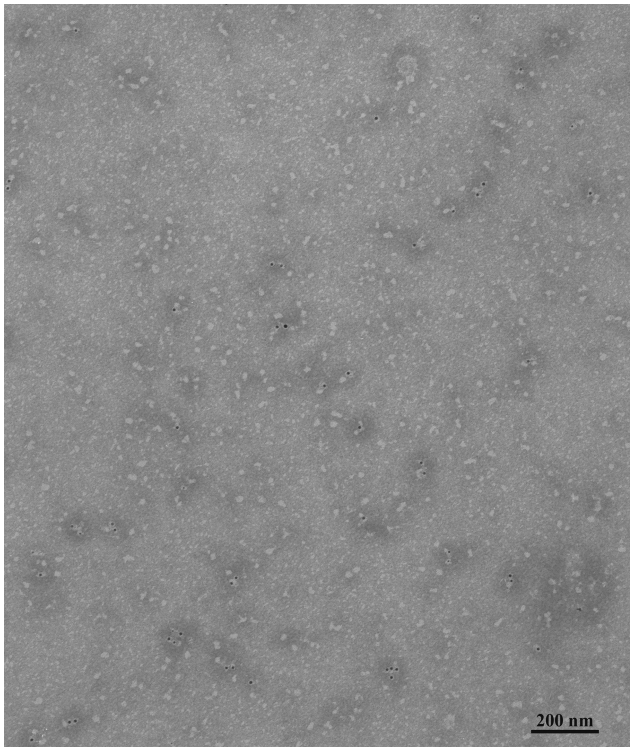

Fig. 8. Low-magnification field of immunolabeled, negatively stained soluble material present in the 17S peak fraction of the gradient.

on the basis of the lengths of their longitudinal and transverse axes. Particles sizes clustered into a few discrete peaks (Fig. 9A). Since within each peak particles exhibited a substantial structural homogeneity, not only in size but also in shape (data not shown), we considered this approach to be tenable and functional for our structural analyses.

Our analysis indicated the occurrence of a dominant peak (in black in Fig. 9A). Particles comprised therein are likely to represent the most stable IFT component. We observed the same size distribution comparing particles labeled with either the IFT139 or the IFT46 antibodies (data not shown). Also, individual particles in the major peak could be labeled by both antibodies (Fig. 9B), indicating that they contain both complex A and complex B polypeptides. These two complexes are known to dissociate after exposure to increased salt concentrations, with the only complex A remaining in the ~16-17S fraction [Lucker et al., 2005]. As a control, we therefore analyzed by negative staining the ~17S fraction obtained after sedimentation in the presence of 300 mM NaCl, the type of particles forming the major peak in Fig. 9A could be no longer visualized (unshown results).

Labeled individual particles are quite similar in appearance to the particles forming the strings we found in the gradient pellet. They are ovoid in shape, about 26 nm × 17 nm in size, and show a thin stem (arrows in Fig. 9B). Thus, both their shape and size are compatible with IFT particles observed in thin sections. The occurrence of a small cavity or cleft on one side (white arrowheads in Fig. 9B) is confirmed in some particles that lie with favourable orientation. Isolated IFT particles were often associated with smaller, elongated elements of variable dimensions (arrowheads in Fig. 9B), which are close in size to the particles in the minor peaks of the size distribution graph, suggesting that these smaller structural elements may be either dissociation products of the IFT particle itself, or part of the interconnecting links.

Thus, the ~17S IFT fraction contains isolated particles showing structural features that are compatible with the size, shape and organization of both the labeled particles found to be associated with the axoneme tip in situ and the particles forming the isolated IFT trains detected in the gradient pellet.

Discussion

In this paper, we show for the first time that IFT particles can be isolated as strings of particles (IFT trains), which can be visualized by negative staining and have been unequivocally identified by labeling with specific antibodies. Moreover, we show that complex A and complex B proteins are present in the same string of particles.

IFT components were originally identified as two protein complexes, A and B, that sedimented on sucrose gradients at ~16-17S and disappeared from flagella of the ts *fla10* mutant after incubation at the restrictive temperature [Kozminski et al., 1995; Piperno and Mead, 1997; Cole et al., 1998]. All the subsequent studies on isolated IFT particles have been focused on samples recovered from the ~16-17S peak fractions of gradients. Biochemical analyses have shown that ~16-17S IFT particles possess a substantial tendency to dissociate into the two complexes A and B, with complex A being more stable than complex B [Cole et al., 1998; Lucker et al., 2005]. Such an intrinsic instability has hampered any approach to the visualization and morphological characterization of isolated, native IFT particles, so that all the ultrastructural information currently available on the IFT system comes from studies on the trains of particles in situ in flat-embedded flagella.

Our biochemical analysis indicates that IFT proteins sediment through the density gradient as two distinct particle populations: one showing the usual sedimentation value of ~16-17S and a second, heavier and fast-sedimenting population, which contains trains of particles that are sometimes (but not always) associated with membrane vesicles. Such a dual sedimentation behaviour has not been reported before. We used mild centrifugation conditions to extract the "soluble" flagellar fraction. Commonly, the insoluble material is removed by low-speed centrifugation, and the soluble supernatant is further clarified by higher-speed centrifugation before it is fractionated through the density gradient [see, e.g., Cole et al., 1998]. The latter step, which is

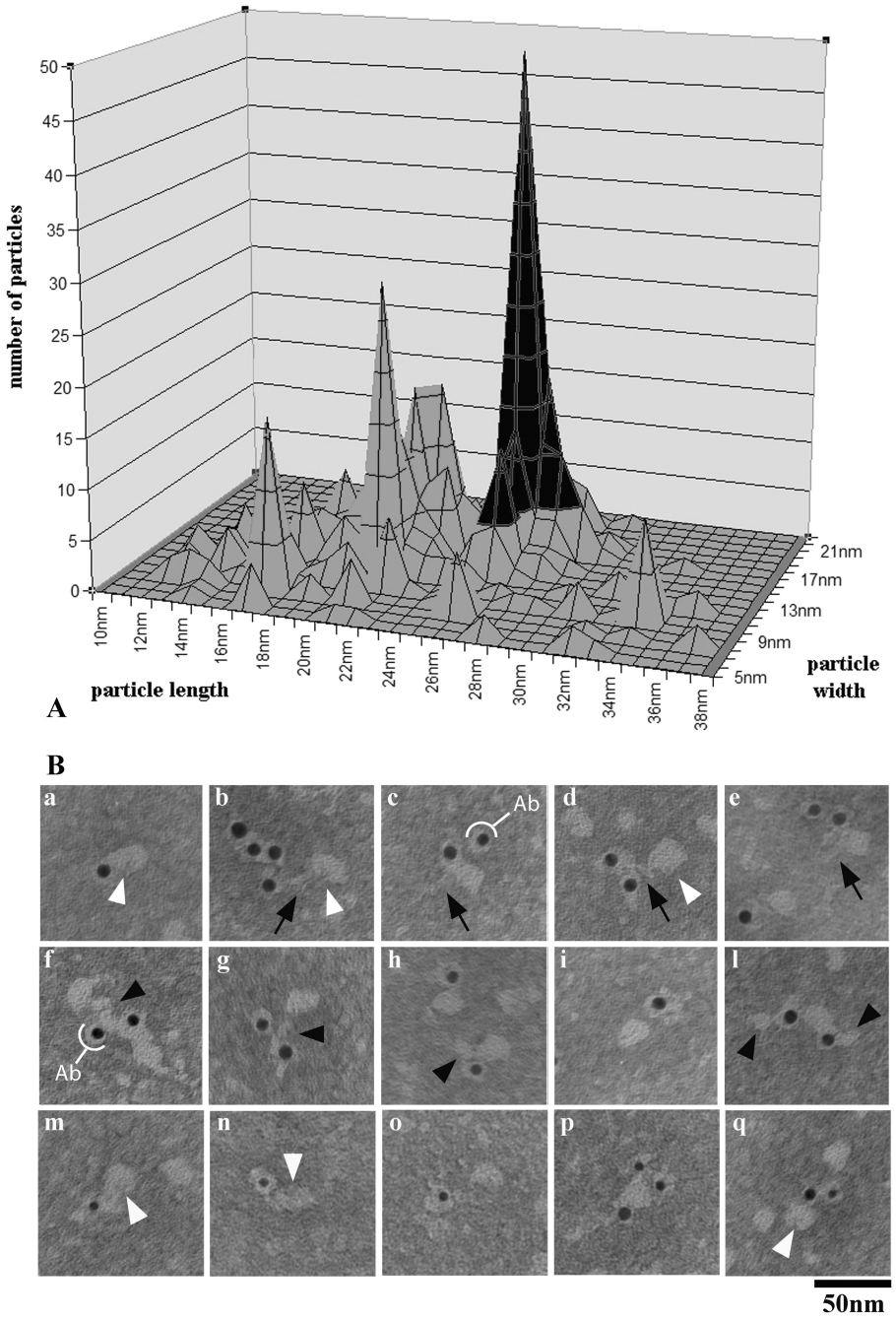

Fig. 9. Immunolabeling of 17S IFT particles. A. Size distribution analysis of labeled, soluble particles occurring in the gradient IFT peak fractions. Both axes (width and length) of each labeled particle were measured; the graph was obtained by plotting the number of counted particles for each pair of length/width values, for a total of 602 soluble particles counted. The graph includes *all* the labeled particles we measured, since no significant difference in the labeling obtained using the IFT46 and the IFT139 antibody was observed. Particles sizes clustered into a few discrete peaks, with the peak in black being the major peak. **B**. Representative, labeled particles from the major peak of the graph shown in A. Particles are labeled by the IFT46 antibody (a–l, 10-nm gold particles), by the IFT139 antibody (m–o, 5-nm gold particles) or by both antibodies (p–q). Ovoid particles, about 26 × 17 nm in size, show a thin stem (black arrows) and a small indentation (white arrowheads), and are often associated with smaller particles (arrowheads). The white semicircles indicate the antibody molecule associated with the gold particle.

likely to remove most of the assembled IFT particles, has been omitted in our protocol.

These experimental conditions allowed us to isolate native IFT particles that are still linked to each other and arranged to form long, flexible strings. This finding indicates that IFT trains do not break down completely after membrane rupture, but are instead able to maintain at least part of their structural organization and some of the interactions linking adjacent particles together. In situ, IFT trains are intimately associated with the flagellar membrane

[Pigino et al., 2009]. Such a close structural juxtaposition suggests that the interaction with the membrane would be required for the ultrastructural integrity of the network of links sustaining IFT organization. This is confirmed by the mild conditions required for the solubilization of IFT trains. However, several free IFT arrays could also be observed that are not associated with membrane vesicles or fragments. This suggests that some of the structural interactions established by IFT particles are not strictly dependent on their association with the membrane.

The strings of particles have been unequivocally identified as part of the IFT system by double immunolabeling with two antibodies, directed either against a complex A or complex B subunit. The distance occurring between the IFT epitope and the gold tag (that can be up to 24 nm) did not allow us to assign each antigen to any definite structure within the string, but we could establish that both complex A and complex B are indeed part of the same train of particles.

Functional studies have indicated that the two complexes play nonoverlapping roles. Mutations affecting complex A lead to a reduced retrograde transport and to the accumulation of complex B polypeptides at the ciliary tip, while defects in most complex B subunits block anterograde movement and result in little or no ciliary assembly [Pazour et al., 2000; Deane et al., 2001; Follit et al., 2006; Absalon et al., 2008; Tsao et al., 2008; Iomini et al., 2001, 2009]. On this basis, complex B and complex A have been related respectively to anterograde and to retrograde IFT transport. However, more recent evidence suggests that the functional roles of the two complexes are not so strictly discernable. In particular, complex A proteins have been shown to be involved in both anterograde and retrograde trafficking and to be required for the localization to cilia of a set of membrane-associated proteins [Mukhopadhyay et al., 2010; Liem et al., 2012].

The two complexes, A and B, have been shown to be independent at the structural level [Cole et al., 1998; Lucker et al., 2005; Behal et al., 2012], but it was suggested that they interact in the flagellar compartment. In fact, complex A and complex B can be coimmunoprecipitated using antibodies against complex B subunits [Qin et al., 2004; Rompolas et al., 2007; Silva et al., 2012], and they enter the flagellum in a stoichiometric amount [Cole et al, 1998]. In a different model organism, the nematode *C. elegans*, the two complexes are transported together during the anterograde movement [Ou et al., 2005, 2007], and the complex A protein IFT144 is required for retrograde transport of complex B components [Wei et al., 2012]. All these data thus indicate that complex A can directly interact with complex B in vivo. Our immunolocalization results are in line with the available information and provide the first direct evidence of the close structural association of the two complexes within the same IFT train.

We could visualize and label IFT particles both in situ, associated with microtubule doublets, or released by whole mount axonemes, and as isolated IFT trains or single particles, and a substantial consistency was observed between the structural features of in situ and isolated particles. The latters appear as ovoid elements whose structure and size fit well with the dimensions and the periodicities previously described for long and short IFT trains [Pigino et al., 2009]. Isolated IFT particles are most frequently found in association with smaller, rod-like elements, which fall into a few dimensional classes. We think it is likely that some of these elements might derive from the dissociation of the interconnecting links, which would constitute weaker structural interaction sites within the IFT train.

In thin sections of embedded flagella, long and short trains have been previously shown to possess distinct architectures, with the short trains being more compact structures, less amenable to ultrastructural analysis [Pigino et al., 2009]. These features are confirmed by our data on demembranated, fixed and whole-mount negatively stained flagella. In addition, such a whole-mount visualization of short trains allowed us to reveal in the short trains the presence of a structurally continuous domain, parallel to the microtubule surface, on which particles are inserted. The occurrence of such a rod-like domain at the interface between the doublet and the rest of IFT train facing the flagellar membrane was suggested by tomographic analysis [Pigino et al., 2009] and is being confirmed by preliminary data from further tomographic analyses of short IFT trains in situ [Lupetti et al., unpublished results]. The functional significance of this domain and its possible relationship to the change in IFT form at the flagellar tip from long to short trains are not yet clear.

The variably long strings of particles we recovered in the gradient pellet should be considered as partially unfolded IFT trains, since they retain some of the ultrastructural features that characterize the IFT trains in situ [Pigino et al., 2009]. These features include (i), the occurrence of links that arrange adjacent particles into linear strings; (ii) the tendency of two linear strings to coalign to form double rows of particles, and, (iii) the ability of IFT trains to interact with the flagellar membrane.

Besides having provided the first images of negatively stained IFT trains and particles and their unequivocal identification by immunolabeling, the possibility to isolate native IFT particles as strings or even double strings opens new opportunities for the high resolution, ultrastructural analyses of IFT trains and their interaction with the membrane.

Materials and Methods

Cell Cultures, Flagella Purification and Fractionation

Chlamydomonas reinhardtii wild type cells were grown vegetatively in liquid minimal medium, M_I, [Sager and Granick, 1953]. Purification of flagella was carried out by the pH

shock procedure as described by Witman et al. [1972] with the minor modifications introduced by Lucker et al. [2005]. Isolated flagella were immediately frozen in liquid nitrogen and stored at −80°C until use. Frozen flagella were left to thaw on ice and were then gently resuspended in HMEK buffer (10 mM HEPES, 5 mM MgSO4, 0.5 mM EDTA, 25 mM KCl, pH 7.2) added with 10 μL/mL plant protease inhibitors (Sigma P9599). The soluble flagellar fraction (membrane + matrix) was obtained by removing the insoluble axonemal fraction by low speed centrifugation at 16000 ×*g* for 10 min at 4°C. The whole supernatant fraction, including the slightly opalescent layer overlying the pellet, was recovered and used for successive immunolabeling and density gradient sedimentation procedures.

Preimmunolabeling and Density Gradient Sedimentation Procedures

The low-speed supernatant (membrane + matrix flagellar fraction) obtained from vegetative flagella as described above, was added with two primary antibodies, the rabbit IFT46 polyclonal antibody, specific for the 46 kDa subunit of IFT complex B, and the mouse IFT139 monoclonal antibody, specific for the 139 kDa subunit of IFT complex A. Both antibodies were added at a 1:40 dilution. The incubation of samples with primary antibodies prior to gradient fractionation was found to result in an increased labeling of IFT particles and in a lower background on electron microscopy grids. After incubation under rocking for 2 hrs at 4°C, ∼350 μL of the preimmunolabeled soluble flagellar fraction were carefully loaded onto 10–30% sucrose gradients (11-mL linear gradients) and centrifuged for 16 hrs at 37,000 rpm using an SW41-Ti rotor (Beckman) at 5°C. Thyroglobulin (19S) and catalase (11S) were used as sedimentation coefficient standards. Control experiments indicated that the binding of primary antibodies did not significantly modify the sedimentation coefficient of ∼17S IFT particles. Gradient fractions of ∼450 μL were collected from the bottom using capillary tubing and a peristaltic pump with a flow rate of 1.5 mL/min. The translucent pellet found at the bottom of the tube was resuspended in 450 μL HMEK buffer and analyzed by electrophoresis, immunoblot and electron microscopy along with all the gradient fractions.

Electrophoresis and Immunoblot

SDS-polyacrylamide gel electrophoresis was carried out according to Laemmli [1970] on 10% acrylamide gels. Proteins were either visualised with Coomassie R-250 or electro-transferred onto nitrocellulose membrane for antibody labeling and detection using the ECL chemiluminescent detection system (GE Healthcare).

Electron Microscopy Procedures

For whole-mount negative staining of flagellar axonemes, a suspension of living cells in HMEK buffer was demembranated and fixed by adding glutaraldehyde and NP-40 at a final concentration of 0.1–0.5% and 0.1%, respectively. After 1 min of incubation, this suspension was diluted 1:10 with HMEK buffer. Cells were allowed to sediment for 2 min onto a 75 mesh, formvar- and carbon-coated grid, and then negatively stained with 1% uranyl acetate.

For in situ immunolabeling of IFT particles, living cells were left to adhere for 5 min onto a formvar and carbon-coated glow-discharged nickel grid, and then exposed for about 30 sec to low-detergent/fixative conditions (0.04% glutaraldehyde, 0.05% NP-40). Grids were successively washed in Tris-buffered saline (TBS) and sequentially incubated as follows: 0.5% bovine serum albumin (1 h), 20 mM glycine (30 min), IFT139 primary antibody (1 h), TBS (3 × 10 min), gold-conjugated secondary antibody (5 nm gold-conjugated anti-mouse IgG, Sigma G7527) (1 h). All these solutions were prepared in TBS. After 5 × 5 min washes in TBS, grids were negatively stained with 1% uranyl acetate.

The pellet and gradient fractions, prelabeled with the primary antibodies (see above) were absorbed on glow-discharged, formvar- and carbon-coated nickel grids for 2–3min. The excess of sample was wiped off, and the grids were processed as described above. The secondary antibody used in this set of experiments to localize the rabbit IFT46 antibody was a 10 nm gold-conjugated anti-rabbit IgG (Sigma G7402).

For transmission electron microscopy observations, the material recovered from the gradient pellet was fixed first in 2.5% glutaraldheyde (1 h) and then in 2.5% glutaraldheyde 0.3% tannic acid (90 min), both prepared in 0.05 M Hepes pH 7.2. After extensive washes in buffer, samples were post-fixed in 1% OsO_4, washed with distilled water, and finally dehydrated and embedded in Epon/Araldyte following standard procedures.

Acknowledgments

The authors are grateful to Tatiana Baldari for critical reading of the manuscript. This research was supported by grants Telethon GGP 07269 and PRIN2009JNTZ4L to PL, and NIH GM 14642 to JLR.

References

Absalon S, Blisnick T, Kohl L, Toutirais G, Doré G, Julkowska D, Tavenet A, Bastin P. 2008 Intraflagellar transport and functional analysis of genes required for flagellum formation in trypanosomes. Mol Biol Cell 19:929–944.

Avidor-Reiss T, Maer AM, Koundakjian E, Polyanovsky A, Keil T, Subramaniam S, Zuker CS. 2004. Decoding cilia function: defining specialized genes required for compartmentalized cilia biogenesis. Cell 117:527–539.

Badano JL, Mitsuma N, Beales PL, Katsanis N. 2006. The ciliopathies: an emerging class of human genetic disorders. Annu Rev Genomics Hum Genet7:125–148.

Baldari CT, Rosenbaum J. 2010. Intraflagellar tran sport: it's not just for cilia anymore. Curr Opin Cell Biol 22:75–80.

Baker SA, Freeman K, Luby-Phelps K, Pazour GJ, Besharse JC. 2003. IFT20 links kinesin II with a mammalian intraflagellar transport complex that is conserved in motile flagella and sensory cilia. J Biol Chem 278:34211–34218.

Behal RH, Miller MS, Qin H, Lucker BF, Jones A, Cole DG. 2012. Subunit interactions and organization of the *Chlamydomonas reinhardtii* intraflagellar transport complex A proteins. J Biol Chem 287:11689–11703.

Bhogaraju S, Taschner M, Morawetz M, Basquin C, Lorentzen E. 2011. Crystal structure of the intraflagellar transport complex 25/27. EMBO J 30:1907–1918.

Cole DG. 2003. The intraflagellar transport machinery of *Chlamydomonas reinhardtii*. Traffic 4:435–442.

Cole DG, Diener DR, Himelblau AL, Beech PL, Fuster JC, Rosenbaum JL. 1998. *Chlamydomonas* kinesin-II-dependent intraflagellar transport (IFT): IFT particles contain proteins required for ciliary assembly in *Caenorhabditis elegans* sensory neurons. J Cell Biol 141:993–1008.

Davis EE, Katsanis N. 2012. The ciliopathies: a transitional model into systems biology of human genetic disease. Curr Opin Genet Dev 22:290–303.

Deane JA, Cole DG, Seeley ES, Diener DR, Rosenbaum JL. 2001. Localization of intraflagellar transport protein IFT52 identifies basal body transitional fibers as the docking site for IFT particles. Curr Biol 11:1586–1590.

Dentler W. 2005. Intraflagellar transport (IFT) during assembly and disassembly of *Chlamydomonas* flagella. J Cell Biol 170:649–659.

Fan ZC, Behal RH, Geimer S, Wang Z, Williamson SM, Zhang H, Cole DG, Qin H. 2010. *Chlamydomonas* IFT70/CrDYF-1 is a core component of IFT particle complex B and is required for flagellar assembly. Mol Biol Cell 21:2696–2706.

Finetti F, Paccani SR, Riparbelli MG, Giacomello E, Perinetti G, Pazour GJ, Rosenbaum JL, Baldari CT. 2009. Intraflagellar transport is required for polarized recycling of the TCR/CD3 complex to the immune synapse. Nat Cell Biol 11:1332–1339.

Follit JA, Tuft RA, Fogarty KE, Pazour GJ. 2006. The intraflagellar transport protein IFT20 is associated with the Golgi complex and is required for cilia assembly. Mol Biol Cell 17:3781–3792.

Hou Y, Qin H, Follit JA, Pazour GJ, Rosenbaum JL, Witman GB. 2007. Functional analysis of an individual IFT protein: IFT46 is required for transport of outer dynein arms into flagella. J Cell Biol 176:653–665.

Huang K, Diener DR, Mitchell A, Pazour GJ, Witman GB, Rosenbaum JL. 2007. Function and dynamics of PKD2 in *Chlamydomonas reinhardtii* flagella. J Cell Biol 179:501–514.

Iomini C, Babaev-Khaimov V, Sassaroli M, Piperno G. 2001. Protein particles in *Chlamydomonas* flagella undergo a transport cycle consisting of four phases. J Cell Biol 153:13–24.

Iomini C, Li L, Esparza JM, Dutcher SK. 2009. Retrograde intraflagellar transport mutants identify complex A proteins with multiple genetic interactions in *Chlamydomonas reinhardtii*. Genetics 183:885–896.

Ishikawa H, Marshall WF. 2011. Ciliogenesis: building the cell's antenna. Nat Rev Mol Cell Biol 12:222–234.

Jékely G, Arendt D. 2006. Evolution of intraflagellar transport from coated vesicles and autogenous origin of the eukaryotic cilium. Bioessays 28:191–198.

Liem KF, Ashe A, He M, Satir P, Moran J, Beier D, Wicking C, Anderson KV. 2012. The IFT-A complex regulates Shh signaling through cilia structure and membrane protein trafficking. J Cell Biol 197:789–800.

Kozminski KG, Johnson KA, Forscher P, Rosenbaum JL. 1993. A motility in the eukaryotic flagellum unrelated to flagellar beating. Proc Natl Acad Sci USA 90:5519–5523.

Kozminski KG, Beech PL, Rosenbaum JL. 1995. The *Chlamydomonas* kinesin-like protein FLA10 is involved in motility associated with the flagellar membrane. J Cell Biol 131:1517–1527.

Laemmli UK. 1970. Cleavage of structural proteins during the assembly of the head of bacteriophage T4. Nature 227:680–685.

Li JB, Gerdes JM, Haycraft CJ, Fan Y, Teslovich TM, May-Simera H, Li H, Blacque OE, Li L, Leitch CC, Lewis RA, Green JS, Parfrey PS, Leroux MR, Davidson WS, Beales PL, Guay-Woodford LM, Yoder BK, Stormo GD, Katsanis N, Dutcher SK. 2004. Comparative genomics identifies a flagellar and basal body proteome that includes the BBS5 human disease gene. Cell 117:541–552.

Lucker BF, Behal RH, Qin H, Siron LC, Taggart WD, Rosenbaum JL, Cole DG. 2005. Characterization of the intraflagellar transport complex B core: direct interaction of the IFT81 and IFT74/72 subunits. J Biol Chem 280:27688–27696.

Lucker BF, Miller MS, Dziedzic SA, Blackmarr PT, Cole DG. 2010. Direct interactions of intraflagellar transport complex B proteins IFT88, IFT52, and IFT46. J Biol Chem 285:21508–21518.

Mukhopadhyay S, Wen X, Chih B, Nelson CD, Lane WS, Scales SJ, Jackson PK. 2010. TULP3 bridges the IFT-A complex and membrane phosphoinositides to promote trafficking of G protein-coupled receptors into primary cilia. Genes Dev 24:2180–2193.

Ou G, Blacque OE, Snow JJ, Leroux MR, Scholey JM. 2005. Functional coordination of intraflagellar transport motors. Nature 436:583–587.

Ou G, Koga M, Blacque OE, Murayama T, Ohshima Y, Schafer JC, Li C, Yoder BK, Leroux MR, Scholey JM. 2007. Sensory ciliogenesis in *Caenorhabditis elegans*: assignment of IFT components into distinct modules based on transport and phenotypic profiles. Mol Biol Cell 18:1554–1569.

Pazour GJ, Wilkerson CG, Witman GB. 1998. A dynein light chain is essential for the retrograde particle movement of intraflagellar transport (IFT). J Cell Biol 141:979–992.

Pazour GJ, Dickert BL, Witman GB. 1999. The DHC1b (DHC2) isoform of cytoplasmic dynein is required for flagellar assembly. J Cell Biol 144:473–481.

Pazour GJ, Dickert BL, Vucica Y, Seeley ES, Rosenbaum JL, Witman GB, Cole DG. 2000. *Chlamydomonas* IFT88 and its mouse homologue, polycystic kidney disease gene *tg737*, are required for assembly of cilia and flagella. J Cell Biol 151:709–718.

Pedersen LB, Miller MS, Geimer S, Leitch JM, Rosenbaum JL, Cole DG. 2005. *Chlamydomonas* IFT172 is encoded by FLA11, interacts with CrEB1, and regulates IFT at the flagellar tip. Curr Biol 15:262–266.

Pedersen LB, Geimer S, Rosenbaum JL. 2006. Dissecting the molecular mechanisms of intraflagellar transport in *Chlamydomonas*. Curr Biol 16:450–459.

Pigino G, Geimer S, Lanzavecchia S, Paccagnini E, Cantele F, Diener DR, Rosenbaum JL, Lupetti P. 2009. Electron-tomographic analysis of intraflagellar transport particle trains in situ. J Cell Biol 187:135–148.

Piperno G, Mead K. 1997. Transport of a novel complex in the cytoplasmic matrix of Chlamydomonas flagella. Proc Natl Acad Sci USA 94:4457–4462.

Porter ME, Bower R, Knott JA, Byrd P, Dentler W. 1999. Cytoplasmic dynein heavy chain 1b is required for flagellar assembly in *Chlamydomonas*. Mol Biol Cell 10:693–712.

Qin H, Diener DR, Geimer S, Cole DG, Rosenbaum JL. 2004. Intraflagellar transport (IFT) cargo: IFT transports flagellar precursors to the tip and turnover products to the cell body. J Cell xBiol 164:255–266.

Qin H, Burnette DT, Bae YK, Forscher P, Barr MM, Rosenbaum JL. 2005. Intraflagellar transport is required for the vectorial movement of TRPV channels in the ciliary membrane. Curr Biol 15: 1695–1699.

Rompolas P, Pedersen LB, Patel-King RS, King SM. 2007. *Chlamydomonas* FAP133 is a dynein intermediate chain associated with the retrograde intraflagellar transport motor. J Cell Sci 120: 3653–3665.

Sager R, Granick S. 1953. Nutritional studies with *Chlamydomonas reinhardtii*. Ann NY Acad Sci 56:831–838.

Silva DA, Huang X, Behal RH, Cole DG, Qin H. 2012. The RABL5 homolog IFT22 regulates the cellular pool size and the amount of IFT particles partitioned to the flagellar compartment in *Chlamydomonas reinhardtii*. Cytoskeleton 69:33–48.

Snow JJ, Ou G, Gunnarson AL, Walker MR, Zhou HM, Brust-Mascher I, Scholey JM. 2004. Two anterograde intraflagellar transport motors cooperate to build sensory cilia on *C*. elegans neurons. Nat Cell Biol 6:1109–1113.

Taschner M, Bhogaraju S, Vetter M, Morawetz M, Lorentzen E. 2011. Biochemical mapping of interactions within the intraflagellar transport (IFT) B core complex: IFT52 binds directly to four other IFT-B subunits. J Biol Chem 286:26344–26352.

Taschner M, Bhogaraju S, Lorentzen E. 2012. Architecture and function of IFT complex proteins in ciliogenesis. Differentiation 83:S12–S22.

Tsao C, Gorovsky MA. 2008. Tetrahymena IFT122A is not essential for cilia assembly but plays a role in returning IFT proteins from the ciliary tip to the cell body. J Cell Sci 121:428–436.

van Dam TJ, Townsend MJ, Turk M, Schlessinger A, Sali A, Field MC, Huynen MA. 2013. Evolution of modular intraflagellar transport from a coatomer-like progenitor. Proc Natl Acad Sci USA 110:6943–6948.

van Reeuwijk J, Arts HH, Roepman R. 2011. Scrutinizing ciliopathies by unraveling ciliary interaction networks. Hum Mol Genet 20:R149–R157.

Wei Q, Zhang Y, Li Y, Zhang Q, Ling K, Hu J. 2012. The BBSome controls IFT assembly and turnaround in cilia. Nat Cell Biol 14:950–957.

Wang Z, Fan ZC, Williamson SM, Qin H. 2009. Intraflagellar transport (IFT) protein IFT25 is a phosphoprotein component of IFT complex B and physically interacts with IFT27 in *Chlamydomonas*. PLoS One 4:e5384.

Witman GB, Carlson K, Berliner J, Rosenbaum JL. 1972. *Chlamydomonas* flagella. I. Isolation and electrophoretic analysis of microtubules, matrix, membranes, and mastigonemes. J Cell Biol 54:507–539.